

 $(\text{Sr}_{1-x}\text{Ca}_x)_3\text{Ru}_2\text{O}_7$ SYSTEM: OPTICAL AND ARPES RESULTSA.V. PUCHKOV^{a,*}, M.C. SCHABEL[†], D.N. BASOV^b, T. STARTSEVA^c, G. CAO^d, T. TIMUSK^c and Z.-X. SHEN^a^aDepartment of Applied Physics, Stanford University, Stanford, CA 94305-4045, USA^bDepartment of Physics, University of California at San Diego, La Jolla, CA 92093-0319, USA^cDepartment of Physics and Astronomy, McMaster University, Hamilton, Ontario, Canada L8S 4M1^dNational High Magnetic Field Laboratory, Florida State University, Tallahassee, FL 32310, USA

Abstract—We present results of the first optical and angle-resolved photoemission (ARPES) measurements on the bilayer $(\text{Sr}_{1-x}\text{Ca}_x)_3\text{Ru}_2\text{O}_7$, or (Ca/Sr)327, system. While the real part of optical conductivity, $\sigma_1(\omega)$, of Sr327 is similar to that of the high- T_c cuprates, $\sigma_1(\omega)$ of Ca327 can be described almost entirely by a single broad Drude-like component. The ARPES results show a dramatic change of the low-energy electronic structure with increasing Ca doping from a normal band metal to a narrow-band marginally metallic phase with a critical behavior at $x = 0.33$.
© 1998 Elsevier Science Ltd. All rights reserved

Perovskite ruthenium oxides of the Ruddlesdon–Popper type, $(\text{Sr}/\text{Ca})_{n+1}\text{Ru}_n\text{O}_{3n+1}$, have attracted significant attention due, in part, to the recent discovery of superconductivity in Sr_2RuO_4 (Sr214)[1]. In addition, these materials exhibit a rich variety of magnetic phases[2–5] and bear strong structural resemblance to the cuprate superconductors, with RuO_2 planes taking the place of the CuO_2 planes. Early work focused primarily on the single plane ($n = 1$) and infinite layer ($n = \infty$) materials, with much less attention given to the two-plane $(\text{Sr}/\text{Ca})_3\text{Ru}_2\text{O}_7$, or (Ca/Sr)327, compounds. Recent advances in crystal growth have allowed synthesis of $(\text{Sr}_{1-x}\text{Ca}_x)_3\text{Ru}_2\text{O}_7$ single crystals over the full doping range $x=0$ –[3]. Despite their structural and chemical similarities, the $x = 0$ and $x = 1$ compounds manifest dramatically different magnetic order. Sr327 is known to be a ferromagnet with moments aligned perpendicular to the RuO_2 planes and a Curie temperature of $T_c = 104$ K, whereas Ca327 is an antiferromagnet with a Néel temperature of $T_N = 58$ K and moments aligned within the planes[3]. We report the first optical and angle-resolved photoemission spectroscopy (ARPES) measurements on various members of the $(\text{Sr}_{1-x}\text{Ca}_x)_3\text{Ru}_2\text{O}_7$ series.

Reflectivity measurements performed over the energy range from 50 cm^{-1} to $35\,000\text{ cm}^{-1}$ were used to calculate the complex optical conductivity through Kramers–Kronig analysis[6]. The single crystal samples formed platelets of $1 \times 1\text{ mm}^2$ typical dimension in the a – b plane. Details of the growth and preparation of crystals have been reported elsewhere[3]. For the ARPES

experiments, samples were cleaved in situ in a vacuum better than 5×10^{-11} torr. Photons at $h\nu = 22.4$ eV and at $h\nu = 27.4$ eV were generated on the undulator beamline 5–3 at Stanford Synchrotron Radiation Laboratory (SSRL). The instrument energy resolution was 0.25 meV (2 cm^{-1}) and 40 meV for the optical and ARPES experiments respectively.

$\sigma_1(\omega)$, the real part of the optical conductivity, is plotted for Ca327 and Sr327 in Fig. 1. The low-frequency spectral weight (SW) in Ca327 is principally concentrated in a single, very broad component centered at $\omega = 0$. Adopting terminology from the high- T_c cuprates[6], we term this the mid-infrared (MIR) band. The shape of this MIR component can be fitted with a Drude formula, $\sigma_1(\omega) = \omega_p^2\tau/(4\pi(1 + \omega^2\tau^2))$, where ω_p is the plasma frequency of the carriers and $1/\tau$ is their scattering rate. Numerical values obtained from the fit are $\hbar\omega_p = 26\,600\text{ cm}^{-1}$ and $\hbar/\tau = 6800\text{ cm}^{-1}$. The large value of the scattering rate is indicative of an extremely short mean free path for the carriers. Assuming a typical Fermi velocity of 10^7 – 10^8 cm s^{-1} , one finds a mean free path of $l = 0.8$ – 8 \AA , well below the limit for coherent, bandlike transport. From $\hbar\omega_p = (4\pi ne^2/m^*)^{1/2} = 26\,600\text{ cm}^{-1}$ we obtain a carrier density of $n = 7.8 \times 10^{21}\text{ cm}^{-3}$, assuming that the effective electron mass, m^* , is unrenormalized relative to the bare electron mass, m_e . This in turn corresponds to an effective carrier density of $N_{\text{eff}} = 0.56$ carriers per Ru ion. While most of the optical conductivity of Ca327 is constituted by the MIR component, some sharp structure is found at low energies, $\hbar\omega < 800\text{ cm}^{-1}$. This frequency is close to the upper cutoff of phonon density of states (assuming it is comparable to that of the cuprates), but we believe that the observed features cannot be described by phonons alone. In particular, the observed redistribution of the conductivity SW

*Corresponding author.

†Present address: Department of Physics, University of Oregon, Eugene, OR 97403, USA.

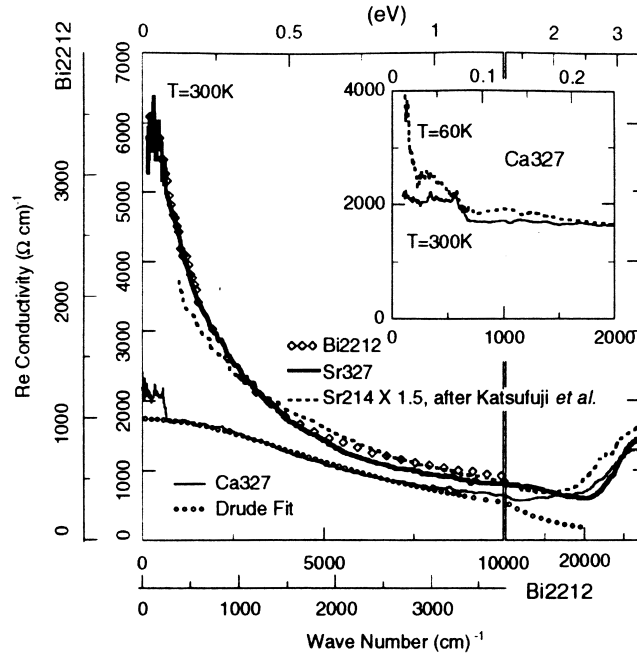


Fig. 1. The optical conductivities of Sr327 and Ca327 taken at room temperature. A Drude fit to the high-energy $\sigma_1(\omega)$ for Ca327 is shown by open circles. The optical conductivity of Sr214 (with the vertical axis rescaled by 1.5) is shown as a dashed line, while $\sigma_1(\omega)$ for optimally doped $\text{Bi}_2\text{Sr}_2\text{CaCu}_2\text{O}_8$ (Bi2212) is shown as open diamonds. For Bi2212 data both axes have been rescaled to show the qualitatively identical frequency dependence for these materials. In the inset the temperature dependence of the low-frequency $\sigma_1(\omega)$ data for Ca327 is plotted.

towards zero frequency with decreasing temperature is reminiscent of free-carrier behavior.[‡]

Comparison of these data with the optical conductivity of Sr327 reveals significant qualitative differences. The low-energy $\sigma_1(\omega)$ is steeply increasing towards zero frequency, suggesting coherent charge transport. Also plotted in Fig. 1 is the optical conductivity for one-plane Sr214[7], rescaled vertically by a factor of 1.5. Clearly, the form of $\sigma_1(\omega)$ in the one- and two-plane materials is essentially identical, suggesting that the interplanar coupling constitutes a relatively weak perturbation, at least at optical energies. The interband optical spectra for all three ruthenate compounds measured ((Sr/Ca)327 and Sr214) show essentially identical behavior at high frequencies, with a peak at around 3 eV. By appropriately rescaling the energy and conductivity axes, it is also possible to superimpose the conductivity curves for Sr327 and the cuprate high- T_c materials on a single curve. This is illustrated in Fig. 1, where $\sigma_1(\omega)$ for optimally doped $\text{Bi}_2\text{Sr}_2\text{CaCu}_2\text{O}_8$ (Bi2212) is plotted as diamonds[8] with the axes scaled to match $\sigma_1(\omega)$ in the $\omega \rightarrow 0$ and $\omega = 10000 \text{ cm}^{-1}$ limits. While absolute dc conductivities are quite similar, the conductivity peak in Sr327 is 2.5 times broader than that of Bi2212. The fact that superconductivity was not observed for Sr327 above

1.7 K[9], and that Sr214 superconducts only at $T < 1 \text{ K}$ [1], suggests that the form of the normal-state optical conductivity is less relevant to the superconducting properties than its absolute width. Using the sum rule, $\omega_p^2 = 8 \int \sigma_1(\omega) d\omega$ [6], we obtain $n = 1.2 \times 10^{22} \text{ cm}^{-3}$, or $N_{\text{eff}} = 0.9$ carriers/Ru, for Sr327. We note that, assuming that each Ru^{4+} ion donates four electrons into conduction bands (which seems to be true for Sr214[10, 11]), one can estimate an average effective mass of these carriers as $m^* = 4/N_{\text{eff}}$. In this way we obtain $m^* \approx 7$ for Ca327 and $m^* \approx 4$ for Sr327. These high values of m^* suggest that strong correlations may be important.

In order to estimate the anisotropy of the electronic transport we have performed optical measurements with polarization of the incident light aligned perpendicular to the RuO_2 planes (which we will refer to as the c -axis direction). Reflectivity of Ca327 along the c -axis as well as perpendicular to this axis is shown in Fig. 2 at room temperature. The anisotropy is evident: while the in-plane reflectivity has a high absolute value, is featureless and rises monotonically towards 100% at zero frequency, the c -axis reflectivity shows much smaller absolute values and sharp features that are due to unscreened phonons. The anisotropy in conductivity can be roughly estimated to be at least a factor of 10.

For the ARPES experiments, crystals with doping levels of $x = 0, 0.33$ were cleaved and measured at $T = 20 \text{ K}$ whereas $x = 1$ crystals were cleaved and measured at $T = 62 \text{ K}$, above the corresponding antiferromagnetic

[‡] $\sigma_1(\omega)$ in the $\omega \rightarrow 0$ limit for both materials is higher than the values obtained in the direct resistivity measurements[3]. However, while optical experiments probe bulk properties, dc resistivity measurements may be affected by surface imperfections.

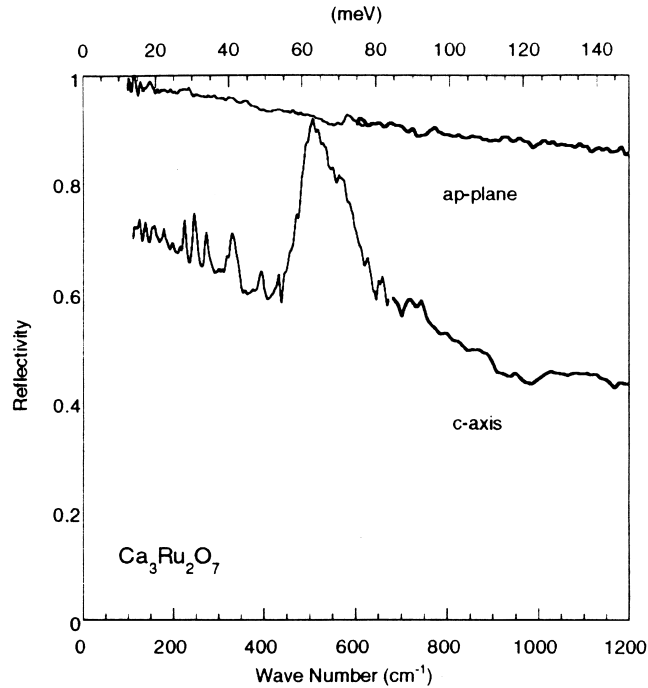


Fig. 2. Reflectivity of Ca327 along the c -axis and perpendicular to the c -axis. The anisotropy of electronic transport is evident.

(AFM) ordering transition[3]. Measured valence band spectra were normalized to the total integrated intensity in the 0–10 eV binding energy window, whereas the low-energy high-resolution spectra were normalized to the corresponding valence band EDCs. Due to space limitations, we present spectra from only a few \mathbf{k} -points. Additional data taken over much more extensive \mathbf{k} grids validate

the conclusions presented here. The large transport anisotropy allows us to neglect the interlayer dispersion and to use a 2D formula $|\mathbf{k}| = [2m(h\nu - E_b - E_v)]^{1/2} \sin \theta$, where E_b is the binding energy, E_v is the work function and θ is the electron emission angle[12].

The angle-resolved spectra for (Ca/Sr)327, obtained along the $(0, 0)$ to (π, π) cut, are shown in Fig. 3 for

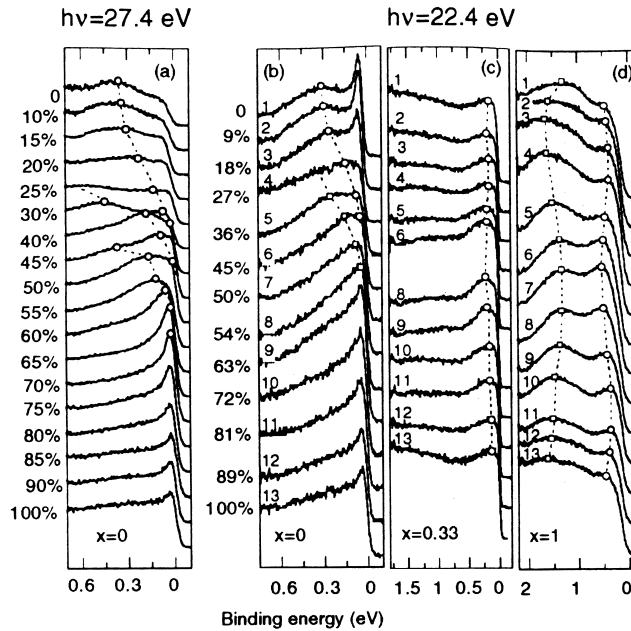


Fig. 3. ARPES results for the members of the $\text{Ca}_x\text{Sr}_{1-x}\text{Ru}_2\text{O}_7$ series along the $(0, 0)$ – (π, π) cut. The spectra were obtained at $h\nu = 27.4$ eV (panel (a)) and $h\nu = 22.4$ eV (panels (b)–(d)). Open symbols mark some of the dispersive features. Numbers on the left show the position in \mathbf{k} -space along the $(0, 0)$ – (π, π) cut, starting at $(0, 0)$. Note that the 50% spectrum for $x = 0.33$ is missing. Also note a difference in energy scales.

several Ca concentrations. The spectra were obtained at photon energies $h\nu = 22.4$ for $x = 0, 0.33, 1$ as well as at $h\nu = 27.4$ for $x = 0$. The spectra are distinguished by relatively high intensity at or near the Fermi energy, a flat region up to the onset of the main valence band, and, for the Sr327 compounds, the presence of a sharp feature near Γ at low binding energy. As is seen in panels 3a and 3b, the sharp feature is very sensitive to the photon energy, being significantly suppressed in the spectra taken at $h\nu = 27.4$ eV. Also, it shows a complete lack of any dispersion. This behavior is reminiscent to that of a surface-related feature observed in $\text{YBa}_2\text{Cu}_3\text{O}_{6.9}$ [13]. Also, its extreme narrowness is uncharacteristic of quasiparticles normally observed in correlated materials, hinting that this peak may be surface derived. Presently the exact origin of this feature remains unresolved and is under further investigation. A comparatively broad peak in Sr327 lying about 350 meV below E_F at Γ , showing clear dispersion along the $(0, 0) - (\pi, \pi)$ line in the two-dimensional Brillouin zone in panels 3a and 3b, appears to correspond to the bottom of an upwardly dispersive conduction band. A second dispersive feature visible in Fig. 3a and 3b corresponds to a second conduction band centered at the Γ -point. While these two bands give rise to two electron-like pieces of the Fermi surface, there exists a third dispersive feature in Sr327, not clearly visible in Fig. 3b but more pronounced in Fig. 3a. This third band gives rise to a hole pocket centered at (π, π) .

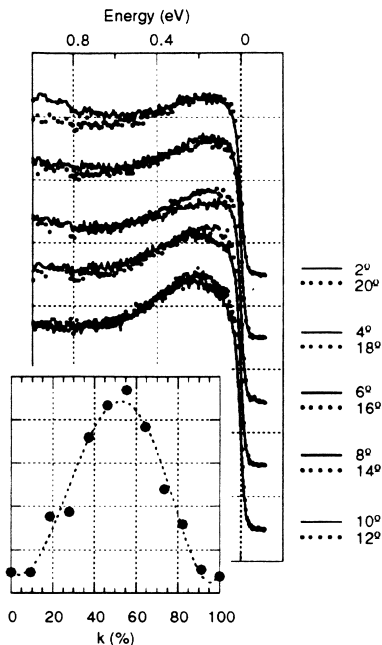


Fig. 4. EDC spectra obtained along the $(0, 0) - (\pi, \pi)$ cut, superimposed in pairs symmetrically around the $(\pi/2, \pi/2)$ point (or approximately 11°). Note a close match between EDCs in the pairs. Inset: ARPES spectral weight, integrated in a binding energy window from -0.1 eV to 0.5 eV, plotted against position along the $(0, 0)$ to (π, π) diagonal. Again, the symmetry is evident.

Qualitatively, the band structure and Fermi surface topology of Sr327 are similar to those calculated within the LDA for Sr214[14], although there are some interesting differences between the two which will be presented elsewhere.

As is seen in Fig. 3c, the spectral features observed in the $x = 0.33$ sample are almost non-dispersive and the higher energy peak is hardly visible. This may be the signature of disorder, but is clearly not a consequence of surface degradation since valence band spectra still exhibit a clear dispersion. In the $x = 1$ material there is an additional feature at about 1.2–1.5 eV. Both features in the $x = 1$ material are dispersive, although the magnitude of that dispersion is still small. A particularly interesting observation in this material is that dispersion of the 500 meV feature appears nearly symmetrical about $(\pi/2, \pi/2)$ along the $(0, 0) - (\pi, \pi)$ line, behavior consistent with Brillouin zone folding due to antiferromagnetic order. Such anti-ferromagnetic ordering has been observed in Ca327 below the Néel temperature $T_N = 58$ K[3, 4]. Because our spectra were taken above T_N , at $T = 62$ K, we conclude that antiferromagnetic fluctuations may persist above T_N . In fact, while a clear dispersion could not be observed for the $x = 0.33$ material, it is interesting that the spectra themselves are symmetrical about $\mathbf{k} = (\pi/2, \pi/2)$, as illustrated in Fig. 4. Indeed, $x = 0.33$ marks the Ca concentration where magnetic moments, aligned ferromagnetically perpendicular to the RuO_2 planes at $x = 0$, start aligning themselves antiferromagnetically in-plane[3]. The ARPES spectra for Ca327 are remarkably similar to those for Ca214[15], which is a real insulator with activated behavior of dc resistivity[2]. The only difference is that the ARPES SW in Ca214 is slightly shifted away from the Fermi energy. Therefore, one may call Ca327 a ‘marginal’ metal since even a slight shift of the ARPES SW away from E_F would make it an insulator.

The high-resolution EDCs from $(\text{Ca}/\text{Sr})327$ show remarkable similarities to those of the cuprate superconductors. In particular, below 2 eV binding energy the SW forms a flat ‘foot’ with clearly visible dispersive features[16].§ The natural separation of the MIR conductivity from the coherent conductivity in Ca327 makes it tempting to search for a similar dichotomy in the ARPES data. While a detailed description of the photoemission lineshape has eluded theory so far, a phenomenological comparison between the optical and ARPES data provides some illuminating insights. To start with, while Sr327 ARPES spectra show strong dispersive features close to the Fermi energy, those for Ca327 do

§In a conventional 2D system the high binding energy tail of a photoemission peak is expected to fall off as a power of $1/\omega$ ($1/\omega^2$ for a Fermi liquid). In the cuprate superconductors (and Sr327) this dependence is much slower, forming a flat ‘background’, or ‘foot’, near E_F .

not. From the optical data, there is only a tiny coherent component in the Ca327 $\sigma_1(\omega)$ spectra, whereas in Sr327 the coherent part of $\sigma_1(\omega)$ is a significant fraction of the total SW. Therefore, a coherent part in the $\sigma_1(\omega)$ spectra can be clearly traced to the dispersive band-like features in ARPES spectra near E_F . Assignment of the MIR band is considerably more difficult. One can start with the experimental fact that the MIR part of $\sigma_1(\omega)$ in both Sr327 and Ca327 is very broad and therefore the charge transport is not band-like (i.e., \mathbf{k} is a 'bad' quantum number). Therefore, one must look for a broad dispersionless feature in the low-energy ARPES spectra. The flat-foot region (or part of it) seems to be the only choice in the case of Sr327. For Ca327, both the ~ 0.5 eV and ~ 1.2 eV as well as the possible 'masked' flat-foot region fit the description. Naïvely, based on the similarities between the optical conductivity of Sr327 and Ca327 at the mid-infrared frequencies, one would expect the ARPES feature associated with the MIR band in $\sigma_1(\omega)$ to look similar in both Sr327 and Ca327. This would suggest that the flat-foot part of the ARPES spectra is an intrinsic feature associated with the MIR component in the optical conductivity. However, one should be careful in making connections between features observed in photoemission and optical experiments since the nature of creating electronic excitations is different for the two techniques: in optical experiments the total number of electrons remains constant, whereas in photoemission experiments one electron is taken out of a system.

In conclusion, we have performed the first optical and ARPES measurements on the (Ca_xSr_{1-x})₃Ru₂O₇ system at doping levels $x = 0, 0.33, 1$. The optical conductivities are similar in the mid-infrared energy range. However, while $\sigma_1(\omega)$ spectra for Sr327 show a significant coherent component appearing qualitatively similar to those of the optimally doped high- T_c oxides, the Ca327 $\sigma_1(\omega)$ spectra show negligible coherent contribution. In agreement with this, strongly dispersive features were observed near E_F in the ARPES spectra of Sr327 which were entirely absent in Ca327. Using ARPES to study the progressive evolution of the low-energy electronic structure of (Ca_xSr_{1-x})₃Ru₂O₇ with doping, we observe a transition

from a band metal to a marginally metallic narrow-band phase, with critical behavior around $x = 0.33$. These findings are in accord with results of recent magnetic and transport measurements[3].

Finally, similarities in both the optical and ARPES results from (Ca/Sr)327 to those of the high- T_c compounds suggest that our results may supply an important insight into the study of high- T_c superconductivity. In particular, the similarities observed at optical and ARPES energy ranges, together with a large difference in superconducting transition temperatures between the ruthenates and the cuprates, suggest that one should probably look at lower energy scales in a hope to find features characteristic of the high- T_c cuprates only.

Acknowledgements—We should like to acknowledge useful discussions with A.J. Berlinsky, J.E. Crow, M. Grainer, K. Kallin, R.B. Laughlin and G.A. Sawatzky. SSRL is operated by the DOE office of Basic Energy Science, Division of Chemical Sciences. The Stanford work is also supported by NSF Grant DMR-93-11566. The work in Florida State University was supported by NSF Cooperative Agreement DMR-95-27035 and the State of Florida. The work in McMaster University was supported by the Natural Science and Engineering Research Council and by the Canadian Institute for Advanced Research. M.C.S. would like to acknowledge the support of the Fannie and John Hertz Foundation.

REFERENCES

1. Maeno, Y. et al., *Nature*, 1994, **372**, 532.
2. Nakatsuji, S. et al., *J. Phys. Soc. Jpn*, 1997, **66**(7).
3. Cao, G. et al., *Phys. Rev. B*, 1997 (to be published).
4. Cao, G. et al., *Phys. Rev. Lett.*, 1997, **78**, 1751.
5. Kanbayasi, A. et al., *J. Phys. Soc. Jpn*, 1976, **41**, 1876.
6. Timusk, T. and Tanner, D.B., in *Infrared Properties of High T_c Superconductors*, ed. I.D.M. Ginsberg. World Scientific, Singapore, 1989, p. 339.
7. Katsufuji, T. et al., *Phys. Rev. Lett.*, 1996, **76**, 126.
8. Puchkov, A.V., Basov, D.N. and Timusk, T., *J. Phys.: Condens. Matter*, 1996, **8**, 10049.
9. Cao, G., private communication.
10. Mackenzie, A.P. et al., *Phys. Rev. Lett.*, 1996, **76**, 3786.
11. Yokoya, T. et al., *Phys. Rev. Lett.*, 1997, **78**, 2272.
12. Himpsel, F.J., *Adv. Phys.*, 1983, **32**, 1.
13. Schabel, M.C. et al., *Phys. Rev. B*, 1997 (submitted).
14. Oguchi, T., *Phys. Rev. B*, 1995, **51**, 1385.
15. Puchkov, A.V. et al. (unpublished).
16. Shen, Z.X. and Dessau, D.S., *Physics Reports*, 1995, **253**, 1.